Check for updates

Effect of pressure on slit channels in guanine sodium salt hydrate: a link to nucleobase intermolecular interactions†

Anna A. Gaydamaka, [iD] *[a] Sergey G. Arkhipov, [iD] [ab] Boris A. Zakharov, [iD] [ab] Yurii V. Seryotkin [iD] [ac] and Elena V. Boldyreva [iD] *[ab]

The crystal structure of a hydrate of the sodium salt of guanine ($2Na^+ \cdot C_5H_3N_5O^{2-} \cdot 7H_2O$) was studied using single-crystal X-ray diffraction and Raman spectroscopy up to ~2.5 GPa, after which the structure distorted and the diffraction pattern from single crystal fragments disappeared along with the appearance of powder ring fragments. On increasing the pressure the distances between the double walls of the slit channels formed by the guanine moieties became more equal, with the longer one shortening and the shorter one expanding. The topology of the Na^+–water intra-channel infinite clusters was preserved, although these clusters became distorted on compression. Among several types of OH···O and OH···N hydrogen bonds, only two practically did not change with increasing pressure, namely the bonds connecting the guanine walls to the intra-channel water molecules. A possible relationship to the interactions in the ion channels with the walls formed by the guanine species in biological systems is discussed.

Introduction

Study of biological and biomimetic systems is important not only for fundamental science but also for the design of drugs and materials. High-pressure research related to biological applications is a rapidly developing field.[1] Most studies are carried out in solutions, but also crystalline materials can serve as biomimetic models.[2] Pressure is an important thermodynamic and kinetic variable. There are several basic reasons why it can be desirable to carry out high-pressure experiments. (i) They allow one to separate thermal and volume effects. (ii) The use of pressure allows one to change, in a controlled way, the intermolecular interactions. This is important, since noncovalent interactions play a primary role in the stabilization of biochemical systems. (iii) Pressure affects chemical equilibria and reaction rates.[3] High pressure is a powerful tool to study experimentally the response of selected hydrogen bonds to mechanical stress in relation to the anisotropy of strain, conformational transitions and compressibility.[4] Theoretical and experimental studies of conformational transitions in biomolecules are of primary importance: conformational transitions in biological molecules are necessary for their normal functioning; at the same time, abnormal conformations may lead to the malfunction of the biomolecules, and result in fatal diseases. High pressure makes it possible to access high-energy conformational states, which play the primary role in the functioning of biomolecules *in vivo*. High pressure can result in conformational transitions, which account for the adaptation of piezophiles to their extreme living conditions,[5] or even in denaturation that is used for the inactivation of pathogens (viruses and bacteria) in medicine and in the food industry.[6–8]

Investigation of macromolecules is challenging. Crystals of smaller fragments of peptides – amino acids – are therefore often studied, in order to obtain quantitative information on the effect of pressure on selected hydrogen bonds and motions of the intramolecular fragments.[2,9–14] Crystals made of small RNA or DNA fragments can serve to model the effect of pressure on nucleic acids and oligonucleotides, similar to how the crystals of amino acids are used to model the properties of peptides. However, nucleic acids, nucleobases, or their derivatives are significantly less studied at high-pressures than amino acids and peptides.[15–20] Nucleic bases and nucleosides were studied mostly by vibrational spectroscopy, whereas only one X-ray diffraction study has been reported.[15] Fourme *et al.* have investigated the behavior of

[a] *Novosibirsk State University, Pirogova Str. 2, Novosibirsk, 630090 Russia.*
E-mail: eboldyreva@yahoo.com
[b] *Boreskov Institute of Catalysis SB RAS, Lavrentieva Ave. 5, Novosibirsk, 630090 Russia*
[c] *Sobolev Institute of Geology and Mineralogy, Koptyuga Ave. 3, Novosibirsk, 630090 Russia*

the d(GGTATACC) oligonucleotide in the range from ambient pressure to 2 GPa. It was shown that the oligonucleotide undergoes remarkable adaptation to high pressure. Such structures could withstand not only the pressure in the deepest sea trenches but also much higher pressures found in the Earth's interior or in the context of rare events such as the impact of a meteorite. Above 1.6 GPa, the compressibility of the oligonucleotide was negative because of super-hydration, *i.e.* incorporation of extra water molecules into the crystal structure, in line with a similar phenomenon found in porous structures, like zeolites compressed in penetrating pressure-transmitting media.[21-23]

Pressure-induced phase transitions at 4–4.5 GPa have been reported for adenosine,[16] deoxyadenosine,[19] cytidine,[17] and deoxycytidine.[18] These transitions are believed to involve changes mainly in the sugar ring. Moreover, from a comparison of the data for adenosine[16] and deoxyadenosine,[19] authors have concluded that deoxyribose is more "flexible" than ribose and, as a result, DNA exhibits conformational flexibility. A high-pressure infrared and Raman spectroscopy study of DNA nucleobases was reported recently.[20] It was shown that all these nucleobases (adenine, guanine, cytosine, and thymine) undergo a phase transition near 2–3 GPa. The reported results are of obvious interest, but additional studies using single-crystal X-ray diffraction are necessary.

Among all the nucleobases, guanine and its analogues are of special importance. Guanine is a purine base present both in DNA and RNA.[24] In addition to this, guanine plays a major role as a structural constituent of second messenger cGMP.[25] It has been suggested in an earlier work[26] that studies of the crystal structures of guanine hydrates can provide significant information on the interactions of water with guanine and its role in DNA mutations.[27-29]

A unique feature of guanine is the ability of the repeat tracts of guanine bases to form tetraplex structures (G-quadruplexes) in the presence of a variety of monovalent cations. In both DNA and RNA, stretches of guanine bases can form stable four-stranded helices in the presence of sodium or potassium ions.[30] Evidence suggests that guanine tetraplexes have important functions within chromosomal telomeres, immunoglobulin switch regions, and the human immunodeficiency virus genome.[31,32] Guanine tetrads have been proposed as building blocks for molecular nanowires for nanoelectronics.[33] Lipophilic helical G-quadruplexes were studied as artificial ion channels.[34] The effect of pressure on the guanine tetraplexes in the presence of various cations and small molecules like urea and trimethylamine *N*-oxide has been studied in solutions in relation to the adaptive mechanisms of deep sea organisms.[35,36] Pressure control of fluorescence emission of thiazole orange (TO) on human telomeric G-quadruplex DNA (h-telo) has been demonstrated to develop a novel DNA nanotechnology, namely a new logic gate system using pressure changes.[37] The structure of a parallel-stranded tetraplex was shown to be stabilized by sodium cations. Sharply resolved sodium cations were found between planes of hydrogen-bonded guanine quartets, and an ordered groove hydration was observed.[31]

To model the effect of pressure on the guanine species in the presence of sodium cations and water molecules we have selected disodium 2-amino-6-oxo-6,7-dihydro-1*H*-purine-1,7-diide heptahydrate. This salt forms single crystals suitable for X-ray diffraction. The structure of this compound has been previously studied by single-crystal X-ray diffraction at ambient pressure (CCDC Refcode YOZPEK).[38] It consists of alternating double layers of guanine anions and hydrated Na^+ cations,[38] so that well-ordered sodium cations and water molecules are located within slit ion channels with guanine walls.

Experimental

Samples

The crystals of disodium 2-amino-6-oxo-6,7-dihydro-1*H*-purine-1,7-diide heptahydrate were synthesized by slow evaporation of aqueous solutions containing guanine (Sigma-Aldrich) and an excess amount of sodium hydroxide (pH ∼ 14) at room temperature.[38] Unfortunately, crystals were prone to form twins and druses. The crystals were unstable under ambient conditions, losing water easily. Therefore, a crystal removed from solution was coated with oil, to avoid complete crystal dehydration.

High pressure generation and measurement

Hydrostatic pressure was generated in diamond-anvil cells (DAC) of 'Almax–Boehler' type without beryllium backing plates[39] with either natural diamonds (suitable both for X-ray diffraction and for Raman experiments) or with synthetic diamonds (suitable for X-ray diffraction only). Either paraffin (ROTH GmbH, hydrostatic limit ∼2 GPa) or a 1:1 stoichiometric pentane–isopentane mixture (hydrostatic limit 7 GPa) was used as a pressure-transmitting medium.[40] Since pentane and isopentane boil at 309 and 301 K, respectively, a special chamber was used to facilitate the DAC loading.[41] The ruby fluorescence method was used for pressure calibration,[42,43] with a precision of 0.05 GPa.

Single-crystal X-ray diffraction

Data were collected using an Oxford Diffraction Gemini R Ultra X-ray diffractometer with a CCD area detector and Mo Kα radiation.

Diffraction data for a free crystal (with a size of 0.23 × 0.06 × 0.05 mm) used in subsequent DAC loading with the pentane–isopentane mixture were collected without a DAC at a MiTeGen polymer sample holder.

The initial crystal structure model for refinement was taken from single-crystal diffraction data under ambient conditions (CCDC 1049453, Refcode YOZPEK).[38] The following software was used: CrysAlis PRO 1.171.38.43d[44] for data

collection, cell refinement, and data reduction; SHELXL-2018/3[45] and ShelXle[46] for structure refinement.

Preliminary experiments were carried out in the pressure range of 0.2–1.9 GPa using paraffin as a pressure transmitting medium. The sample was not a single crystal, but a multi-twin crystal. The data reduction was carried out using only one orientation matrix. However, the quality of data was not high enough to refine the atomic coordinates with high precision. Therefore, we do not present here the full data for the single crystal X-ray diffraction experiments carried out in paraffin, and report only the changes in unit cell parameters. A better set of diffraction data could be obtained from a better crystal in the pressure range of 0–2.5 GPa using pentane–isopentane (1:1) as pressure transmitting media. In general, the results obtained in the two series of experiments with the two pressure-transmitting media agreed well, with the data obtained with pentane–isopentane being of higher quality.

Absorption of X-rays with the sample for a free crystal was taken into account using CrysAlis PRO[44] (analytical absorption correction). Absorption of X-rays with the diamonds and the sample in high-pressure experiments was taken into account using ABSORB7 (Gaussian absorption correction).[47] The reflections from the sample which overlapped with diamond and gasket reflections were excluded manually.

For the free crystal all non-H atoms were refined in an anisotropic approximation. H-Atom parameters in the CH group were constrained using AFIX 43 with $U_{iso}(H) = 1.2U_{eq}(C)$, and those in the NH$_2$ group were constrained using AFIX 93 with $U_{iso}(H) = 1.2U_{eq}(N)$. H-Atoms belonging to water molecules were refined freely. For high pressure data, all non-H atoms were refined in isotropic approximation. H-Atom parameters in the CH group were constrained using AFIX 43 with $U_{iso}(H) = 1.2U_{eq}(C)$, and those in the NH$_2$ group were constrained using AFIX 93 with $U_{iso}(H) = 1.2U_{eq}(CN)$. H-Atoms belonging to water molecules were not recognized and not refined.

Mercury 3.10[48] and Vesta[49] were used for structure visualization and analysis. STRAIN[50] was used to calculate the anisotropy of lattice strain.

Raman spectroscopy

Raman experiments were performed for the sample loaded in paraffin in parallel with X-ray diffraction, to obtain additional information. Raman spectra were recorded using a LabRam HR 300 spectrometer from HORIBA Jobin Yvon with a CCD detector. For spectral excitation a 488 nm line of an Ar$^+$ laser was used with a beam size of ~1 μm at the surface of the sample and a power of ~8 mW. All data were collected using a Raman microscope in a backscattering geometry. The spectral resolution was ~2 cm^{-1}. At each pressure point (up to 2.5 GPa), after X-ray diffraction data collection, a Raman spectrum without polarization of scattered beam was recorded besides pressure point at 1.9 GPa, after which the pressure in

the DAC was increased and Raman spectra measurement was repeated at the next pressure point. A number of spectra were recorded on pressure release. A Raman spectrum for the free crystal was also recorded.

Results and discussion

Details of data collection for the sample in paraffin are summarized in Table S1.† Details of data collection, structure solution and refinement for the sample in pentane–isopentane are summarized in Table S2.† The data on the crystal structure at ambient pressure agreed well with previously reported results.[38] Structural data are deposited at the Cambridge Structural Data Center (Refcodes CCDC 1904141–1904147).

The asymmetric unit with the immediate contacts (hydrogen bonds) is plotted in Fig. 1. The crystal structure of the guanine sodium salt hydrate can be described as a series of parallel slit channels with the walls formed from double layers of guanine anions and the inner part filled with sodium cations of two different types and water molecules (Fig. 2). There are no hydrogen bonds between guanine anions. This contrasts with the guanine species in many biological structures, as well as anhydrous guanine[51,52] or guanine monohydrate,[53] but resembles (in this respect) some other salt hydrates, e.g. guaninium dinitrate dihydrate.[54]

The neighbouring guanine anions are located in the planes parallel to each other, to form dimers shifted with respect to each other along the [011] direction (Fig. 2b and 3a). The distances between the planes, in which the neighbouring
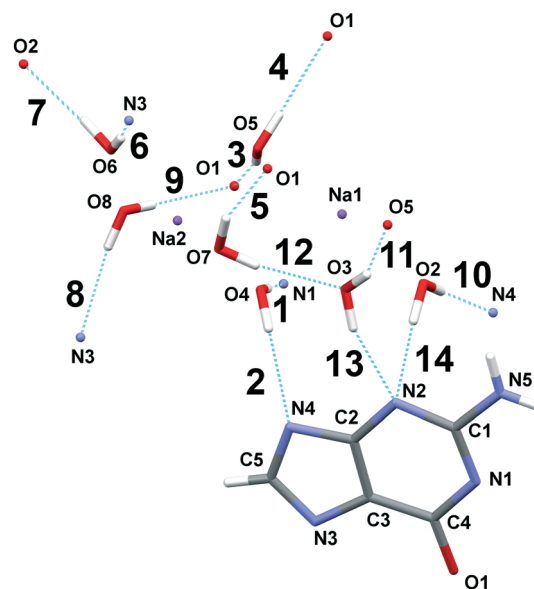

Fig. 1 The asymmetric unit of disodium 2-amino-6-oxo-6,7-dihydro-1H-purine-1,7-diide heptahydrate with the immediate contacts (hydrogen bonds). The numbering of atoms is the same as in CIF for CCDC 1049453 based on a previous publication.[38] Dotted blue lines show hydrogen bonds. The numbering of hydrogen bonds is the same throughout the text.
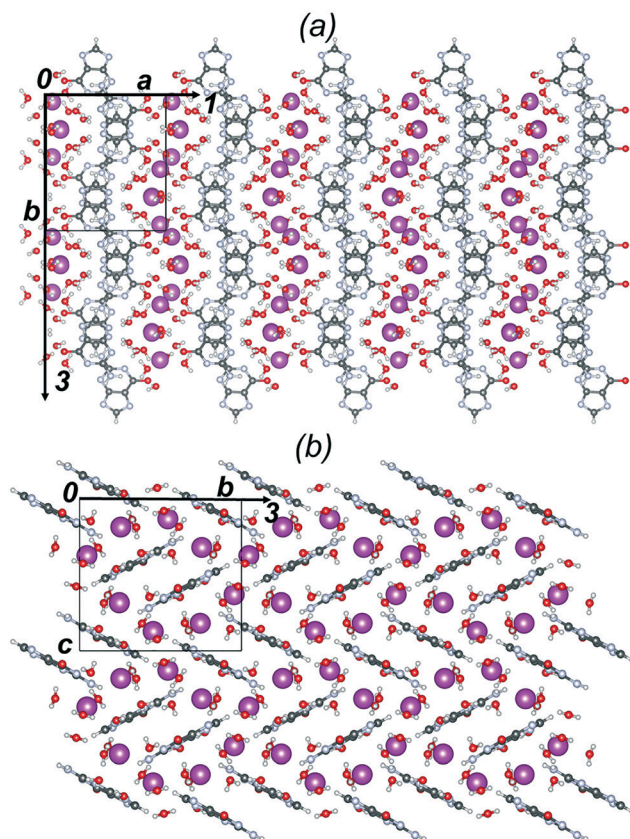
Fig. 2 (a) The crystal structure viewed down the *c* axis, showing the alternating layers of guanine anions and hydrated sodium cations. (b) A view down the *a* axis showing the herringbone crystal packing motif, including edge-to-face interactions between the guanine anion dimers. Numbers 1–3 show the direction of the corresponding axes of the strain ellipsoid (1 is the direction of minimum compression, 3 is the direction of maximum compression, 2 is normal to the plot).

guanine anions are located, are equal at ambient pressure to 3.474 Å (I) and 2.014 Å (II) (Fig. 3). There are two symmetry related systems of parallel planes. For comparison, in the structure of the guanine monohydrate all the guanine molecules are stacked along the *c* axis with an interplanar spacing of 3.30 Å.[53] The base-pair spacing in the DNA of A and B types is equal to 2.925 Å and 3.35 Å, respectively.[15] Sodium cations and water molecules are ordered and are involved in multiple directional interactions with each other (Fig. 4 and Tables S3 and S4†). The OH···O and OH···N hydrogen bonds of different types link water molecules with each other and also to the guanine anions (Fig. 1 and Table S5†). Trial experiments on hydrostatic compression were carried out with paraffin as a pressure-transmitting fluid. The changes in unit cell parameters and volume were continuous until ~2.4 GPa (Fig. S1†). In the range between 1.9 and 2.4 GPa stripes appeared on the crystal surface, although the crystal shape was preserved (Fig. 5a). The diffraction pattern changed: the reflections split, suggesting that the single crystal was destroyed, to form several domains. The Raman spectra also changed, confirming that a phase transformation took place (Fig. 6). The lattice parameters at 2.4 GPa were refined; how-
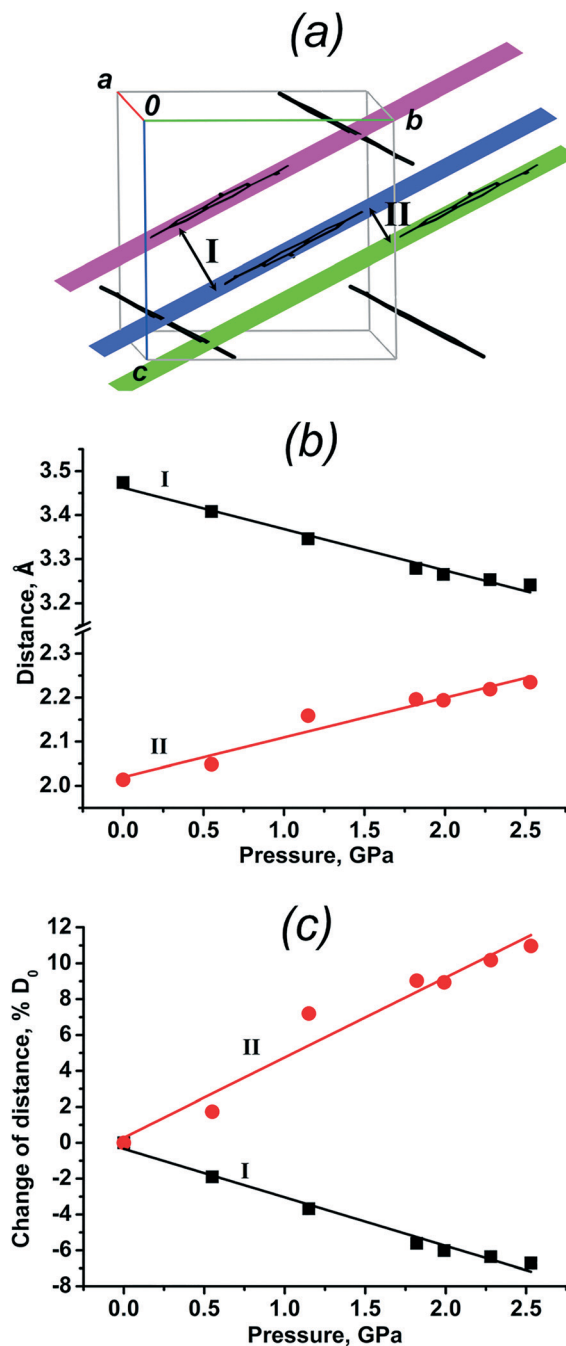

Fig. 3 (a) Alternating planes corresponding to the neighbouring guanine anions. Numbers I and II indicate long and short distances between the planes, respectively. (b) Distances between guanine rings; (c) relative changes of these distances.

ever, the R_{int} value was high (37.6%), and reliable intensity measurement was not possible, therefore atomic coordinates could not be found. After pressure release the crystal was non-transparent and its diffraction pattern remained very poor; the Raman spectra indicated that the phase transition was structurally reversible, although accompanied with crystal disintegration.

Since the phase transition point practically coincided with the hydrostatic limit of paraffin, it could be supposed that
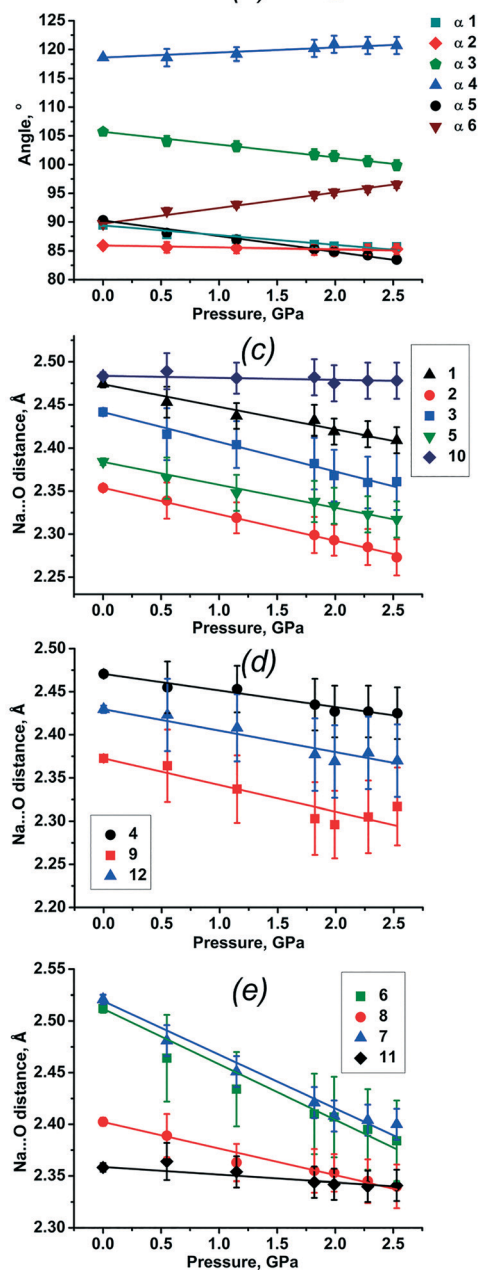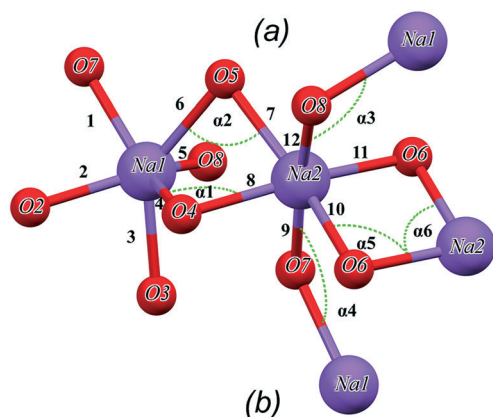
Fig. 4 (a) A fragment of the unit cell showing Na···O distances and selected angles. The numbering of bonds and angles is the same throughout the text. (b) Selected angles vs. pressure. (c–e) Distances between Na and O atoms vs. pressure.
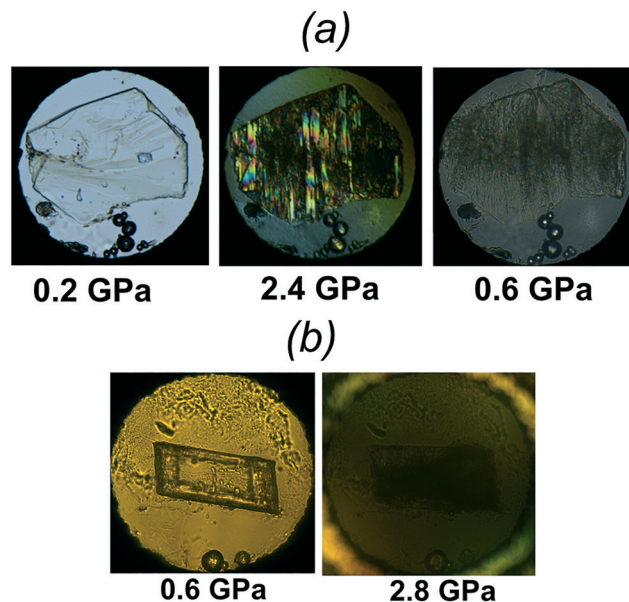

Fig. 5 Photos of the crystals in paraffin (a) and pentane–isopentane (b).

the phase transition was facilitated by shear stresses. In order to test if a phase transition occurs also under hydrostatic compression, we have carried out the second experiment with a 1:1 stoichiometric pentane–isopentane mixture (hydrostatic limit 7 GPa). The dependence of unit cell parameters and volume on pressure agreed reasonably well with that observed in the experiments with paraffin (Fig. S1†). A phase transition did occur also in this medium, though at a pressure slightly higher than that in the experiments with paraffin (between 2.5 and 2.8 GPa). The crystal habit did not change (Fig. 5b), but the crystal became opaque, and the X-ray diffraction pattern deteriorated drastically; the single-crystal reflections disappeared and only fragments of powder rings could be observed. A number of powder ring fragments became visible on the last runs of the data set collected at 2.5 GPa.

The volume decrease on compression from 1 atm to 2.5 GPa was ~10.9%. The compression was strongly anisotropic (Fig. 2 and 7): a minimum linear compression (close to zero) was observed normal to the slit channels, whereas the compression within the layers of the slit channels was higher, with a maximum linear compression (-6.5% on the pressure increase from 1 atm to 2.5 GPa; -2.6% GPa^{-1}) – along the b axis, i.e. along the axis of a channel (Fig. 2a and 7). For comparison, the typical values of relative volume change that have been reported earlier for crystalline amino acids are about -5% GPa^{-1} (-1% GPa^{-1} for proteins), and crystal structures often undergo phase transitions, when the volume decrease without a phase transition can be ~3.5–15% and even larger (20–30%) for such robust structures as α-glycine or DL-serine.[2,9,11–14]

The effect of pressure on various types of intermolecular interactions in the crystal structure is remarkable. The distances between the planes, in which the guanine anions were
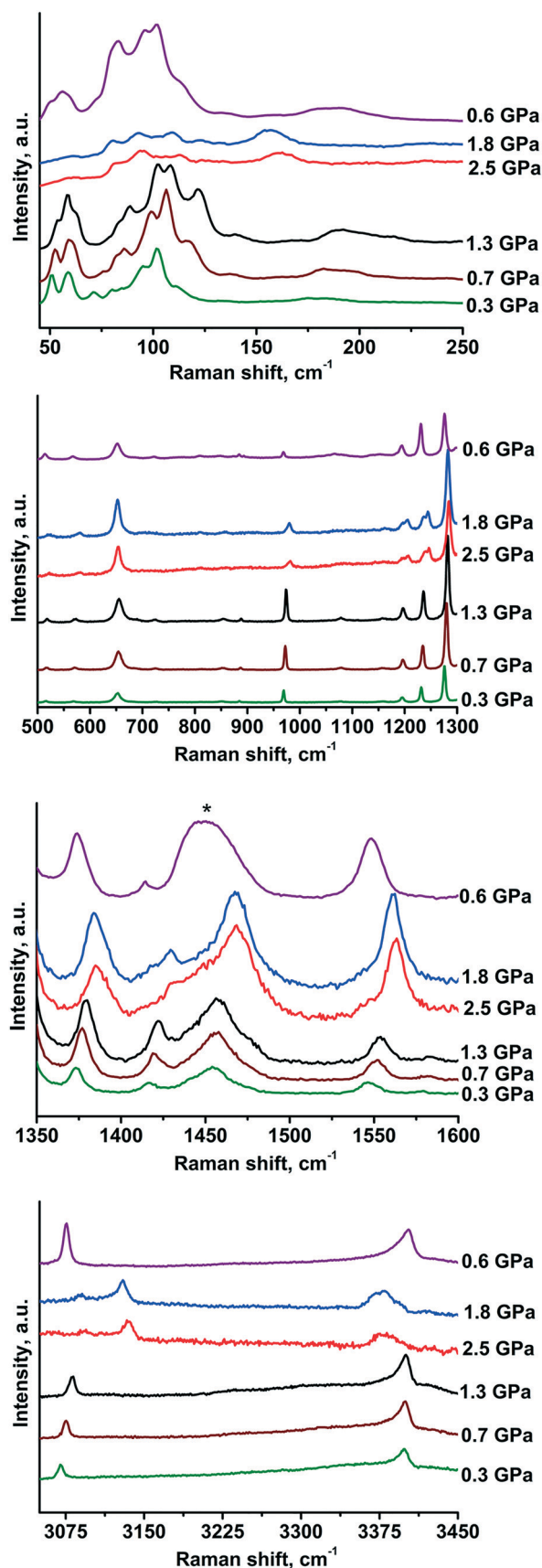
Fig. 7 Linear strain in the directions of the principal axes of the strain ellipsoid for the title salt. 1 is the direction of minimum compression, 3 is the direction of maximum compression.

Fig. 6 Raman spectra of the title salt at multiple pressures (0.3–2.5 GPa – increase of pressure, 2.5–0.6 GPa – decrease of pressure). The band from media is indicated by an asterisk (*).
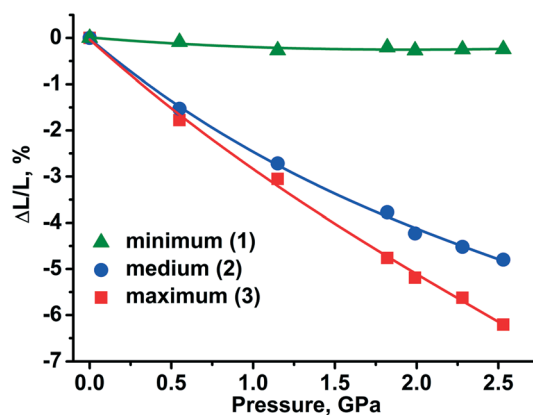
located, became more equal on compression, with the longer one shortening and the shorter one expanding (Fig. 3). The relative changes in these distances were +0.09 Å GPa^{-1} (+4.34% GPa^{-1}) for the short one and −0.09 Å GPa^{-1} (−2.65% GPa^{-1}) for the long one. For comparison, the distances between the nucleotide heterocycles in the crystalline models of the DNA A and DNA B changed on compression at −0.11 Å GPa^{-1} and −0.15 Å GPa^{-1} (−3.74% GPa^{-1} and −4.48% GPa^{-1}), respectively.[15] Interestingly, the crystal structures of the d(GGTATACC) oligonucleotide mimicking the DNA A and DNA B fragments collapsed at pressures ∼2 GPa (similar to this work), when the base-pair spacing reached 2.75 Å and 3.35 Å.[15] The decrease in the differences in the distances between the neighbouring atoms or molecular fragments is often observed with increasing pressure; extension of selective individual bonds makes it possible to achieve a closer packing of all the chemical species in a crystal structure and in this way, to minimize the free energy of the system as a whole.[4,55–62]

The topology of the Na$^+$–water clusters in the inner space of the slit channels (Fig. 4a) did not change with increasing pressure, though the Na$^+$–OH$_2$ distances and the Na$^+$–O–Na$^+$ angles changed significantly (Fig. 4b–e and Tables S2 and S3 and Movie S1 in the ESI†).

Among several types of OH⋯O and OH⋯N hydrogen bonds, only two practically did not change with increasing pressure, namely the hydrogen bonds connecting the guanine walls with the intra-channel water molecules (Table S5† and Fig. 1 and 8).

The changes in the interactions with increasing pressure manifested themselves in the Raman spectra (Fig. 6). The phase transition is clearly visible in the pressure range between 1.3 and 2.5 GPa. The most pronounced discontinuous changes are related to low-wavenumber translation and libration bands (50–200 cm^{-1}). The strong intensity decrease and significant broadening of the bands indicate discontinuous lattice distortion. At the same time the high-frequency region of the Raman spectra shows a clear jump of ν(OH) frequencies from 3400 to 3380 cm^{-1} indicating that the distance
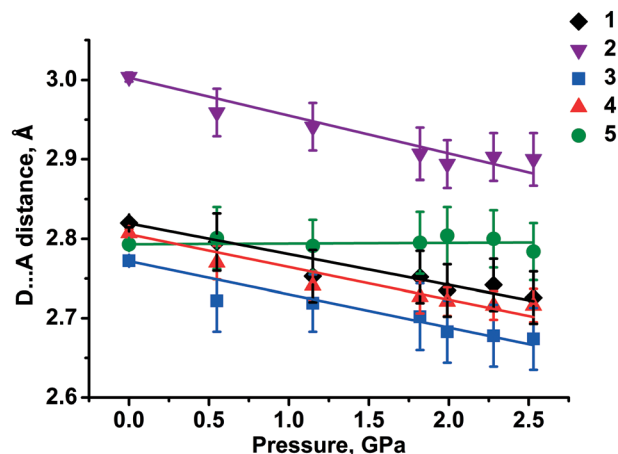
Fig. 8 Distances between non-hydrogen atoms in the selected hydrogen bonds vs. pressure. Numbering is the same as that in Fig. 1 and Table S5.†

between the donor and acceptor atoms in the hydrogen bonds formed by water molecules became shorter. This suggests that these hydrogen bonds became stronger, or even protonation of the guanine dianion at the cost of a hydrogen atom of one of the water molecules occurred. This could be confirmed with the appearance of characteristic N–H modes, but according to ref. 20 they should be active only in the IR-spectra. This leads to further stabilization and hardening of the hydrogen-bonding network within the Na^+–water clusters. In this case the irreversible crystal disintegration can be explained by the fact that a large deformation of Na^+–water clusters within the layers does not match the structural changes in the layered walls formed by the guanine moieties which are only weakly bound by non-covalent interactions. In the spectrum of the low-pressure phase this band does not shift with increasing pressure from 0.3 to 1.3 GPa, while most of the bands slightly shift to higher wavenumbers (indicating that the distances between atoms, which are not involved in hydrogen bonding, became shorter). The Raman spectra at 1.9 GPa were not recorded. However, the trend of $\nu(OH)$ vibration frequency changes at pressures up to 1.3 GPa did not suggest that a dramatic change could occur at 2.5 GPa, if no phase transition took place. The band splitting of the C–H in-plane bending (1197 cm^{-1} at 1.3 GPa, 1195 cm^{-1} and 1205 cm^{-1} at 2.5 GPa) and C–NH_2 stretching (1235 cm^{-1} at 1.3 GPa, 1240 cm^{-1} and 1246 cm^{-1} at 2.5 GPa) modes accompanying the phase transition may be a sign of crystal symmetry lowering. The jumpwise changes in the interactions between the guanine anions manifest themselves additionally by discontinuous changes in the intramolecular vibrations of guanine anions on phase transition. The most pronounced changes are detected for $\nu(C–H)$ (from 3081 to 3134 cm^{-1}) and $\nu(C=C)$ (from 1553 to 1563 cm^{-1}).

The phase transition in this pressure range is also in agreement with the X-ray diffraction data. The structural rearrangement appeared to be large enough to cause the crystal fragmentation. The structural changes were only partly reversible on decompression; this manifested itself in the broadening of the Raman bands that were preserved on pressure release even at 0.6 GPa, even though the positions of the bands on decompression were restored as they were in the initial crystal before the pressure increase. This irreversible broadening of all Raman bands can be attributed to the crystal fragmentation, partly irreversible phase transition, or rather partial disordering/amorphization.

The above mentioned changes in the Raman spectra indicate that the phase transition is partially reversible, but is accompanied by crystal disintegration, and possible symmetry lowering.

These observations suggest that the layered crystal structure of this hydrated sodium salt of guanine is in fact stabilized by the interactions between the guanine host "double walls" and the well-structured sodium cation–water guests filling the slit channels. Such a structure withstands pressures up to 2–3 GPa and can be compressed to ∼90% of its initial volume before a significant structural rearrangement occurs.

Conclusions

The importance of various systems containing guanine fragments is so enormous that hundreds of publications are dedicated to their theoretical and experimental studies *in vivo* and *in vitro* in solutions, as well as in the crystalline state. Still, the "enigma of guanine", the "guanigma"[51] is far from being solved. Studies of relatively simple systems, such as the sodium salt hydrate discussed in this work, can shed additional light on the interactions in which guanine is involved, in relation to their optical properties, ionic transport and structural stability to external stimuli like temperature or pressure variations. Other multicomponent crystals with different packings of guanine moieties containing (in addition to guanine) various alkali metal cations, as well as other components can be of interest for biological modelling or for tuning optical properties.

Conflicts of interest

There are no conflicts of interest to declare.

Acknowledgements

Notes and references

1 R. Winter, *Advances in High Pressure Bioscience and Biotechnology II*, Springer-Verlag, Heidelberg, 2003.
2 E. V. Boldyreva, *Model. Myster. Magic Mol.*, 2008, pp. 167–192.

3 D. Lopes, S. Grudzielanek, K. Vogtt and R. Winter, *J. Non-Equilib. Thermodyn.*, 2007, **32**, 41–97.

4 E. V. Boldyreva, in *Understanding Intermolecular Interactions in the Solid State – Approaches and Techniques*, ed. D. Chopra, RSC, 2018, pp. 32–97.

5 *High-Pressure Crystallography. From Novel Experimental Approaches to Applications in Cutting-Edge Technologies*, ed. E. V. Boldyreva and P. Dera, Springer, Dordrecht, 2010, p. 612.

6 D. Farr, *Trends Food Sci. Technol.*, 1990, **1**, 14–16.

7 R. P. Lopes, M. J. Mota, A. M. Gomes, I. Delgadillo and J. A. Saraiva, *Compr. Rev. Food Sci. Food Saf.*, 2018, **17**, 532–555.

8 Y.-M. Zhao, M. de Alba, D.-W. Sun and B. Tiwari, *Crit. Rev. Food Sci. Nutr.*, 2018, 1–15.

9 E. V. Boldyreva, *Acta Crystallogr., Sect. A: Found. Crystallogr.*, 2008, **64**, 218–231.

10 E. V. Boldyreva, *Phase Transitions*, 2009, **82**, 303–321.

11 S. A. Moggach, S. Parsons and P. A. Wood, *Crystallogr. Rev.*, 2008, **14**(2), 143–184.

12 P. T. C. Freire, in: *High-Pressure Crystallography. From Novel Experimental Approaches to Applications in Cutting-Edge Technologies*, ed. E. V. Boldyreva and P. Dera, Springer, Dordrecht, 2010, pp. 559–572.

13 C. H. Görbitz, *Acta Crystallogr., Sect. B: Struct. Sci.*, 1989, **45**, 390–395.

14 C. H. Görbitz, *Crystallogr. Rev.*, 2015, **21**, 160–212.

15 R. Kahn, M. Lecouvey, E. Girard, R. Fourme, E. Migianu-Griffoni, M. Mezouar, A.-C. Dhaussy, T. Prange and J.-C. Chervin, *Nucleic Acids Res.*, 2007, **35**, 4800–4808.

16 K. C. Martin, D. A. Pinnick, S. A. Lee, A. Anderson, W. Smith, R. H. Griffey and V. Mohan, *J. Biomol. Struct. Dyn.*, 1999, **16**, 1159–1167.

17 J. Li, S. A. Lee, D. A. Pinnick, A. Anderson, W. Smith, R. H. Griffey and V. Mohan, *J. Biomol. Struct. Dyn.*, 2002, **19**, 1111–1120.

18 S. A. Lee, I. Lawson, L. Lettress and A. Anderson, *J. Biomol. Struct. Dyn.*, 2006, **23**, 677–684.

19 S. A. Lee, I. Lawson, L. Lettress and A. Anderson, *J. Biomol. Struct. Dyn.*, 2007, **24**, 579–588.

20 S. Y. Yang and I. S. Butler, *J. Biomol. Struct. Dyn.*, 2013, **31**, 1490–1496.

21 Y. Lee, C. C. Kao and T. Vogt, *J. Phys. Chem. C*, 2012, **116**, 3286–3291.

22 D. Seoung, Y. Lee, C. C. Kao, T. Vogt and Y. Lee, *Chem. – Eur. J.*, 2013, **19**, 10876–10883.

23 D. Seoung, Y. Lee, C. C. Kao, T. Vogt and Y. Lee, *Chem. Mater.*, 2015, **27**, 3874–3880.

24 M. Blackburn, M. J. Gait, D. Loakes and D. M. Williams, *Nucleic Acids in Chemistry and Biology*, 3rd edn, 2006.

25 R. P. Lopes, M. P. M. Marques, R. Valero, J. Tomkinson and L. A. E. Batista De Carvalho, *Adv. Biomed. Spectrosc.*, 2013, **7**, 127–145.

26 D. Gur, M. Pierantoni, N. Elool Dov, A. Hirsh, Y. Feldman, S. Weiner and L. Addadi, *Cryst. Growth Des.*, 2016, **16**, 4975–4980.

27 M. S. Cooke, M. D. Evans, M. Dizdaroglu and J. Lunec, *FASEB J.*, 2003, **17**, 1195–1214.

28 H. Kasai, *Mutat. Res.*, 1997, **387**, 147–163.

29 A. Chworos, Y. Coppel, I. Dubey, G. Pratviel and B. Meunier, *J. Am. Chem. Soc.*, 2001, **123**, 5867–5877.

30 D. M. J. Lilley, A. I. H. Murchie, K. Phillips, Z. Dauter and B. Luisi, *J. Mol. Biol.*, 2002, **273**, 171–182.

31 G. Laughlan, A. I. H. Murchie, D. G. Norman, M. H. Moore, P. C. Moody, D. M. Lilley and B. Luisi, *Science*, 1994, **265**, 520–524.

32 G. N. Parkinson, M. P. H. Lee and S. Neidle, *Nature*, 2002, **417**, 876–880.

33 A. B. Kotlyar, N. Borovok, T. Molotsky, H. Cohen, E. Shapir and D. Porath, *Adv. Mater.*, 2005, **17**, 1901–1905.

34 S. L. Forman, J. C. Fettinger, S. Pieraccini, G. Gottarelli and J. T. Davis, *J. Am. Chem. Soc.*, 2000, **122**(17), 4060–4067.

35 R. Winter, J.-M. Knop, S. Patra, B. Harish and C. A. Royer, *Chem. – Eur. J.*, 2018, **24**, 14346–14351.

36 S. Patra, V. Schuabb, I. Kiesel, J. M. Knop, R. Oliva and R. Winter, *Nucleic Acids Res.*, 2019, **47**, 981–996.

37 S. Bhowmik, S. Takahashi and N. Sugimoto, *ACS Omega*, 2019, **4**, 4325–4329.

38 D. Gur and L. J. W. Shimon, *Acta Crystallogr., Sect. E: Crystallogr. Commun.*, 2015, **71**, 281–283.

39 R. Boehler, *Rev. Sci. Instrum.*, 2006, **77**, 2004–2007.

40 G. J. Piermarini, S. Block and J. D. Barnett, *J. Appl. Phys.*, 1973, **44**, 5377–5382.

41 B. A. Zakharov and A. F. Achkasov, *J. Appl. Crystallogr.*, 2013, **46**, 267–269.

42 G. J. Piermarini, S. Block, J. D. Barnett and R. A. Forman, *J. Appl. Phys.*, 1975, **46**, 2774–2780.

43 R. A. Forman, G. J. Piermarini, S. Barnett and J. D. Block, *Science*, 1972, **176**, 285.

44 Rigaku-Oxford Diffraction Ltd, *CrysAlisPRO*, Yarnton, Oxfordshire, England, 2016.

45 G. M. Sheldrick, *Acta Crystallogr., Sect. C: Struct. Chem.*, 2015, **71**, 3–8.

46 C. B. Hübschle, G. M. Sheldrick and B. Dittrich, *J. Appl. Crystallogr.*, 2011, **44**, 1281–1284.

47 R. Angel and J. Gonzalez-Platas, *J. Appl. Crystallogr.*, 2013, **46**, 252–254.

48 C. F. Macrae, I. J. Bruno, J. A. Chisholm, P. R. Edgington, P. McCabe, E. Pidcock, L. Rodriguez-Monge, R. Taylor, J. Van De Streek and P. A. Wood, *J. Appl. Crystallogr.*, 2008, **41**, 466–470.

49 K. Momma and F. Izumi, *J. Appl. Crystallogr.*, 2011, **44**, 1272–1276.

50 Y. Ohashi and C. W. Burnham, *Am. Mineral.*, 1973, **58**, 843–849.

51 A. Hirsch, D. Gur, I. Polishchuk, D. Levy, B. Pokroy, A. J. Cruz-Cabeza, L. Addadi, L. Kronik and L. Leiserowitz, *Chem. Mater.*, 2015, **27**, 8289–8297.

52 K. Guille and W. Clegg, *Acta Crystallogr., Sect. C: Cryst. Struct. Commun.*, 2006, **62**, 515–517.

53 U. Thewalt, C. E. Bugg and R. E. Marsh, *Acta Crystallogr., Sect. B: Struct. Crystallogr. Cryst. Chem.*, 1971, **27**, 2358–2363.

54 K. Bouchouit, N. Benali-Cherif, L. Benguedouar, L. Bendheif and H. Merazig, *Acta Crystallogr., Sect. E: Struct. Rep. Online*, 2002, **58**, o1397–o1399.

55 J. S. Tse and E. V. Boldyreva, in *Modern Charge-Density Analysis*, ed. C. Gatti and P. Macchi, Springer, 2012, vol. XXIII, pp. 573–623.

56 G. Resnati, E. Boldyreva, P. Bombicz and M. Kawano, *IUCrJ*, 2015, **2**, 675–690.

57 E. V. Boldyreva, H. Ahsbahs and H. P. Weber, *Z. Kristallogr.*, 2003, **218**, 231–236.

58 N. Casati, P. Macchi and A. Sironi, *Angew. Chem., Int. Ed.*, 2005, **44**, 7736–7739.

59 N. Casati, P. Macchi and A. Sironi, *Chem. – Eur. J.*, 2009, **15**, 4446–4457.

60 A. Prescimone, C. J. Milios, S. Moggach, J. E. Warren, A. R. Lennie, J. Sanchez-Benitez, K. Kamenev, R. Bircher, M. Murrie, S. Parsons and E. K. Brechin, *Angew. Chem., Int. Ed.*, 2008, **47**, 2828–2831.

61 L. Rechignat, M. Nardone, G. Molnár, A. Bousseksou, T. Guillon, T. Kitazawa and N. O. Moussa, *Chem. Phys. Lett.*, 2006, **423**, 152–156.

62 G. Agustí, A. B. Gaspar, M. C. Muñoz and J. A. Real, *Inorg. Chem.*, 2007, **46**, 9646–9654.